

Generalized Hadamard-Product Fusion Operators for Visual Question Answering

Brendan Duke^{*†}, Graham W. Taylor^{*†‡}

^{*}School of Engineering, University of Guelph

[†]Vector Institute for Artificial Intelligence

[‡]Canadian Institute for Advanced Research

{bduke,gwtaylor}@uoguelph.ca

Abstract—We propose a generalized class of multimodal fusion operators for the task of visual question answering (VQA). We identify generalizations of existing multimodal fusion operators based on the Hadamard product, and show that specific non-trivial instantiations of this generalized fusion operator exhibit superior performance in terms of OpenEnded accuracy on the VQA task. In particular, we introduce Nonlinearity Ensembling, Feature Gating, and post-fusion neural network layers as fusion operator components, culminating in an absolute percentage point improvement of 1.1% on the VQA 2.0 test-dev set over baseline fusion operators, which use the same features as input. We use our findings as evidence that our generalized class of fusion operators could lead to the discovery of even superior task-specific operators when used as a search space in an architecture search over fusion operators.

Index Terms—Model Selection; Visual Question-Answering

I. INTRODUCTION

Multimodal applications offer a challenge to model selection in machine learning, as the interactions between different data modalities (e.g., between video and audio, or between images and questions) may require a complicated prior in order to accurately capture regularities necessary for downstream tasks.

The particular multimodal application that we consider in this work is that of visual question-answering (VQA), i.e., of producing a natural language response to the combined input consisting of an image and a natural language question pertaining specifically to that image. In the case of VQA, the complexity of the task exists in both extracting useful feature representations from the question and the image, as well as the “fusion” of these feature representations by combining them in order to predict the answer to the question. In this paper, we focus on the problem of combining feature representations in the VQA task through models based on a generic “fusion operator” definition.

We illustrate the complexity of model selection for the VQA task by designing a class of multimodal fusion operators, each of which combines raw question and visual data streams to predict answers to the given questions based on an image. We evaluate specific instances of high performing fusion operators belonging to the same design class.

We evaluate and discuss three multimodal fusion architectural components that emerge as improving performance as part of the investigation into the general class of fusion operators:

- 1) The use of a gating mechanism, wherein individual features extracted by the fusion operator are turned on or off by a multiplicative interaction.
- 2) The introduction of distinct nonlinearities between parallel components in the fusion operator, which we hypothesize adds a performance boost due to an ensembling effect.
- 3) The additional introduction of learned nonlinearity in the form of a neural network inside the fusion operator, which takes features from the bilinear interaction of a pair of question and visual feature vectors as input.

II. RELATED WORK

A. Model Selection

We propose that the task of model selection applied to multimodal problem domains can be improved by using automated architecture search techniques. Reinforcement learning has been used to conduct automated search for neural network architectures [1], gradient descent optimizers [2] and activation functions [3]. Other options for architecture search include evolutionary optimization [4], Bayesian optimization [5], and gradient descent-based methods.

We contribute to multimodal model selection by describing a generalized class of fusion operators that can be used as a design space for many of the search techniques described above. We enable future research to bypass the difficult problem of model selection for multimodal applications by using automated model design techniques that use the search space we describe as a basis.

B. Fusion Operators

We focus on multimodal fusion of two modalities, applied to the task of visual question-answering. We use modality to refer to a raw data stream of information, as would be presented to an observer from a sensor. In the case of the VQA application, the first modality is the sentence corresponding to the asked question. The second modality is the image about which the question is being asked.

Current research in multimodal fusion for VQA focuses on performance improvements by approximating a bilinear product between a feature vector \mathbf{q} extracted from the question, and a feature vector \mathbf{v} extracted from the image [6], [7], [8]. The feature vectors \mathbf{q} and \mathbf{v} can be produced by pre-trained feature

extraction methods specific to encoding information from the sentence and image modalities into vector representations.

In the experimental design of this work, as well as in the work of [7] and [8], a pre-trained Residual Network model [9] is used as a feature extractor for the image data stream, and a pre-trained Skip-Thought Vectors [10] model is used to extract features from the sentence data stream.

In general, we define a fusion operator for the VQA task as a function \mathcal{F}_θ , parametrized by θ , of the question feature vector \mathbf{q} and the visual feature vector \mathbf{v} . The fusion operator \mathcal{F}_θ computes a vector output, which is consumed downstream by a function g , e.g. a linear layer followed by a softmax layer, in order to model a probability distribution over the answer y conditional on \mathbf{q} and \mathbf{v} :

$$p(y | \mathbf{q}, \mathbf{v}; \theta) = g(\mathcal{F}_\theta(\mathbf{q}, \mathbf{v})). \quad (1)$$

The methods of [6], [7] and [8] all propose that in the multimodal application of VQA, the outer product of the feature vector \mathbf{q} extracted from the question, with the feature vector \mathbf{v} extracted from the image, produces a more expressive feature representation than straightforward concatenation, element-wise product, or element-wise sum. These previous works design fusion operators based on approximations to the outer product $\mathbf{q} \otimes \mathbf{v}$.

The Multimodal Compact Bilinear Pooling (MCB) method of [6] uses the Compact Bilinear Pooling method of [11] to approximate a bilinear interaction between \mathbf{q} and \mathbf{v} . In the case of MCB, the fusion operator \mathcal{F}_θ consists of projecting \mathbf{q} and \mathbf{v} using Count Sketch [12], followed by convolution of \mathbf{q} and \mathbf{v} , which is done efficiently using an element-wise multiplication in the frequency domain.

The MCB method makes use of the fact that the Count Sketch of the outer product $\Psi(\mathbf{q} \otimes \mathbf{v}, h, s)$, where h and s are uniform random variables as described in [6], is equal in expectation to the convolution $\Psi(\mathbf{q}, h, s) * \Psi(\mathbf{v}, h, s)$ of the question and visual feature representations, i.e., $E[\Psi(\mathbf{q} \otimes \mathbf{v}, h, s)] = E[\Psi(\mathbf{q}, h, s) * \Psi(\mathbf{v}, h, s)]$. However, since this expectation is intractable to compute, [7] proposes a fusion operator based on the Hadamard (element-wise) product.

The fusion operator in [7], the Multimodal Low-rank Bilinear Attention Networks (MLB), uses the Hadamard product coupled with projections of \mathbf{q} and \mathbf{v} with learned weight matrices $W_{\mathbf{q}}$ and $W_{\mathbf{v}}$, in order to make a low-rank approximation to the general outer product $\mathbf{q} \otimes \mathbf{v}$. The projected vectors are multiplied by a third weight matrix $W_{\mathbf{z}}$, such that the fusion operator in the case of MLB is $\mathcal{F}_\theta(\mathbf{q}, \mathbf{v}) = W_{\mathbf{z}}^T(W_{\mathbf{q}}^T \mathbf{q} \odot W_{\mathbf{v}}^T \mathbf{v})$, where \odot denotes the Hadamard product. Combined, the weight matrices $W_{\mathbf{q}}$, $W_{\mathbf{v}}$ and $W_{\mathbf{z}}$ approximate the general weight tensor \mathcal{T} corresponding to the bilinear interaction between \mathbf{q} and \mathbf{v} in the special case where \mathcal{T} is of low rank. The idea of using a constrained-rank weight tensor in the outer product $\mathbf{q} \otimes \mathbf{v}$ is the same idea used in the MUTAN fusion operator of [8], which generalizes MLB by allowing the bilinear interaction tensor between \mathbf{q} and \mathbf{v} to be of rank R .

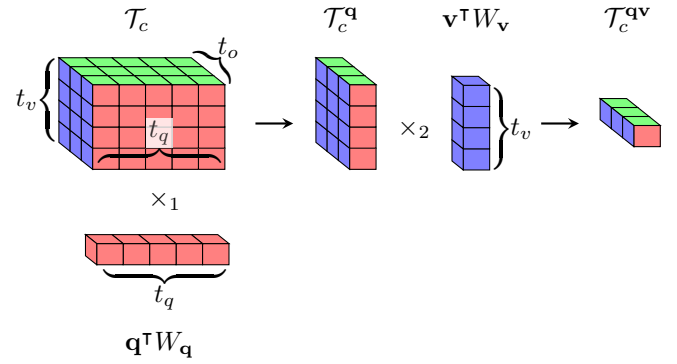


Fig. 1. A geometric representation of the first two n -mode products of the right hand side Tucker decomposition of Equation 3, where $A = \mathbf{q}^T W_{\mathbf{q}}$ and $B = \mathbf{v}^T W_{\mathbf{v}}$, i.e. $\mathcal{T}_c \times_1 \mathbf{q}^T W_{\mathbf{q}} \times_2 \mathbf{v}^T W_{\mathbf{v}}$. From left to right, the vector $\mathbf{q}^T W_{\mathbf{q}}$ is first combined with the core tensor \mathcal{T}_c by taking the inner product along the dimension of size t_q between $\mathbf{q}^T W_{\mathbf{q}}$ and each of the $t_v \times t_o$ fibers composing \mathcal{T}_c , producing the matrix $\mathcal{T}_c^{\mathbf{q}}$. Then, $\mathbf{v}^T W_{\mathbf{v}}$ is combined with $\mathcal{T}_c^{\mathbf{q}}$ by taking the inner product between $\mathbf{v}^T W_{\mathbf{v}}$ and the t_o columns of $\mathcal{T}_c^{\mathbf{q}}$, producing the vector $\mathcal{T}_c^{\mathbf{qv}}$.

MUTAN is a fusion operator that is motivated in [8] by the Tucker decomposition [13], which we discuss in Section II-C. In Section III-B, we derive the form of bilinear interaction used by the MUTAN fusion operator from the definition of the Tucker decomposition, since we base our fusion operator models on this derivation as well. The MUTAN fusion operator generalizes the MLB fusion operator to an interaction tensor of rank R , and therefore is,

$$\mathcal{F}_\theta(\mathbf{q}, \mathbf{v}) = \sum_{r=1}^R W_{\mathbf{z}}^T(W_{\mathbf{q}}^T \mathbf{q} \odot W_{\mathbf{v}}^T \mathbf{v}). \quad (2)$$

C. Tucker Decomposition

The Tucker decomposition is a form of higher-order principal component analysis [13], which decomposes a tensor into a series of three n -mode tensor products between a single core tensor \mathcal{T}_c and three matrices:

$$\mathcal{T} \approx \mathcal{T}_c \times_1 A \times_2 B \times_3 C \quad (3)$$

In Equation 3, the n -mode tensor product denoted by \times_n is the multiplication of a tensor by a matrix, or by a vector, as in the case of MUTAN and our own method.

In general, the n -mode tensor product of a tensor $\mathcal{T} \in \mathbb{R}^{I_1 \times I_2 \times \dots \times I_N}$ with a matrix $W \in \mathbb{R}^{J \times I_n}$ yields a new tensor $\mathcal{T} \times_n W$ with size $I_1 \times \dots \times I_{n-1} \times J \times I_{n+1} \times \dots \times I_N$.

In our special case, where we have an n -mode product between \mathcal{T} and a vector \mathbf{z} , the size of $\mathcal{T} \times_n \mathbf{z}$ becomes $I_1 \times \dots \times I_{n-1} \times 1 \times I_{n+1} \times \dots \times I_N$. The mode- n ‘‘fiber’’, referring to the generalization of rows and columns of matrices to higher-order tensors as defined in [13], $\mathcal{T}_{i_1 \dots i_{n-1} : i_{n+1} \dots i_N}$ of \mathcal{T} along I_n becomes a single element resulting from the dot product of $\mathcal{T}_{i_1 \dots i_{n-1} : i_{n+1} \dots i_N}$ with \mathbf{z} .

Formally, the element-wise definition of the n -mode product between tensor \mathcal{T} and vector \mathbf{z} is:

$$(\mathcal{T} \times_n \mathbf{z})_{i_1 \dots i_{n-1} i_{n+1} \dots i_N} = \sum_{i_n=1}^{I_n} \mathcal{T}_{i_1 \dots i_N} z_{i_n}, \quad (4)$$

where in Equation 4, the dimensionality of $\mathcal{T} \times_n \mathbf{z}$ is reduced to $N - 1$ by summing over the n th dimension. The n -mode product is depicted in Figure 1.

In Section III-B, we use the definition of the Tucker decomposition from Equation 3, along with the definition of the n -mode product for the special case of multiplication between a tensor and a vector, in order to derive the MUTAN fusion operator of Equation 2, and to further generalize the derived fusion operator to include Feature Gating and Nonlinearity Ensembling.

III. METHODS

In this section, we present the methods used to derive a generalization of bilinear fusion operators for the combination of two feature vectors in multimodal applications. We subdivide our methods into the data and model sub-categories of the machine learning process. We first discuss the data used in our experiments, followed by discussion of the fusion operator model and how we generalized the model into a class of fusion operators over which we instantiated and evaluated a range of specific instances.

A. Data

The VQA 1.0 dataset [14] is a dataset of “free-form and open-ended Visual Question Answering (VQA)”. The VQA task is to give an open-ended natural language response to an input consisting of a natural language question and an image. In VQA 1.0, there are 23 234 unique one-word answers for real images, and therefore the model’s outputs can be represented as a multiple choice over these answers. In practice, we limit the number of choices to the top 2000 most common answers in the training dataset.

The VQA 1.0 real images dataset consists of 204K images from the MSCOCO dataset [13], 614K questions, and 6M answers (ten answers per question). The dataset is separated into a 2/1/2 training/validation/test split by the VQA 1.0 authors.

It is known that due to the data collection methodology of the VQA 1.0 dataset, there exists an imbalance in the dataset that allows questions to be answered with high accuracy without taking the image into account; this is remedied with VQA 2.0 [15], which balances the answers to each question, so that the best scores on the VQA 2.0 dataset are not possible using language priors alone.

The balancing of VQA 2.0 is due to the addition of complementary images, wherein for a given image and question pair (I, Q) with answer A , a complementary image I' is found that is similar in appearance, but has a different answer A' to the question. The new example (I', Q, A') is then added to the dataset. VQA 2.0 includes 195K, 93K, and 191K complementary images in the training, validation, and test sets,

respectively. In total, the VQA 2.0 dataset has 443K training, 214K validation, and 453K test (image, question) pairs.

The increased difficulty of the VQA 2.0 dataset with regards to emphasizing the importance of the combination of visual and question features creates a larger gap between relatively strong and weak fusion operators, i.e., the performance gap between strong and weak fusion operators increases when moving from VQA 1.0 to VQA 2.0, even when the absolute performance decreases for both models under consideration [15]. Therefore, we evaluate our proposed fusion operators on VQA 2.0.

B. Model

Following the work of [7] and [8], we represent the sentence and visual modalities with extracted feature vectors. We use a pre-trained Skip-Thought Vectors model [10] to extract a “question vector” feature representation \mathbf{q} from a question. As well, we use a ResNet [9] pre-trained on ImageNet [16] to extract a “visual vector” feature representation \mathbf{v} from an image.

For the purpose of this paper, the Skip-Thought Vectors model and ResNet can each be thought of as “black boxes” used to extract useful feature representations from sentences and images, respectively. By using this black-box abstraction, the fusion operators we develop can automatically benefit from improved feature extraction models without altering the algorithm presented here.

The Skip-Thought Vectors model extracts a d_q vector from the question, and the ResNet model extracts a $d_v \times S \times S$ tensor from the image, where S is the pre-pooling spatial dimension of the feature maps produced by the ResNet.

The MUTAN fusion operator of [8] and MLB fusion operator of [7] combine the image and sentence feature vectors by approximating a bilinear interaction between the vectors. The bilinear interaction is learned, and the output of that interaction is input into a linear predictive layer, which is in turn fed into a softmax layer that outputs probabilities over the top 2000 most common answers in the training data.

We generalize the bilinear interaction of MUTAN and MLB such that both MLB and MUTAN, as well as element-wise multiplication and element-wise addition, can all be represented in a common form.

We derive our fusion operator as a generalization of the MUTAN fusion operator by first deriving MUTAN from the definition of the Tucker decomposition [13], then discussing the generalization of this expression. We begin from the definition of the Tucker decomposition given in Equation 3.

In the case of MUTAN, A in Equation 3 corresponds to the vector $\mathbf{q}^\top W_q \in \mathbb{R}^{1 \times t_q}$, B is $\mathbf{v}^\top W_v \in \mathbb{R}^{1 \times t_v}$, and C is $W_o \in \mathbb{R}^{|A| \times t_o}$, where $|A|$ is the dimensionality of the output vector (i.e., the number of answer classes), and t_q , t_v and t_o are the respective dimensionalities of the vector spaces that the question features, image features, and fused question-image features are projected onto before applying a linear prediction layer W_o .

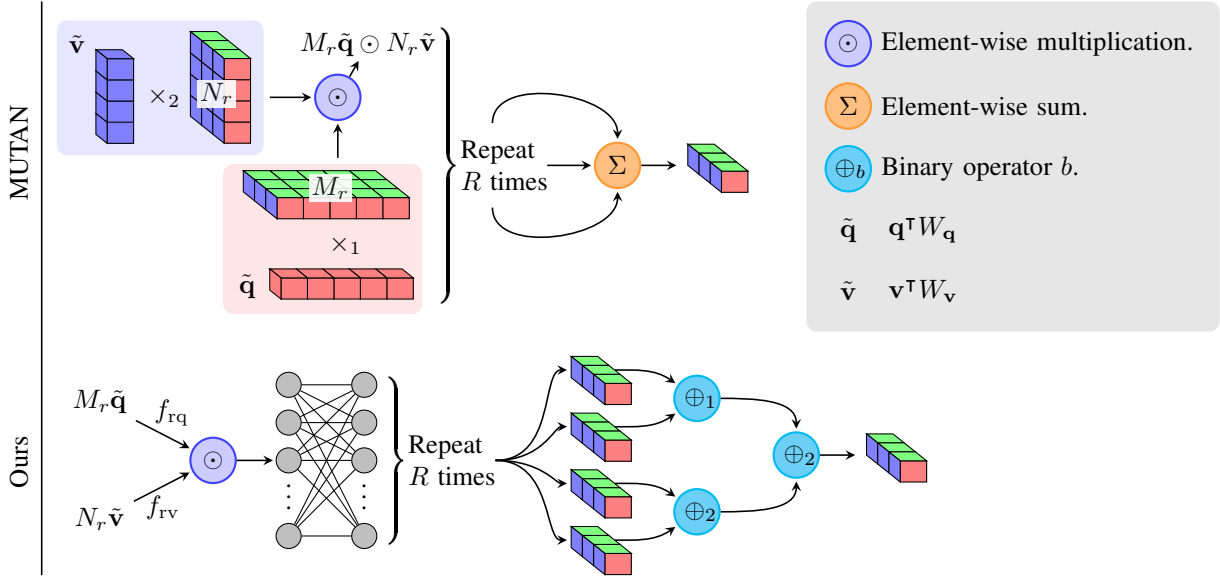


Fig. 2. A comparison between the MUTAN fusion operator of [8] (top) and our generalized fusion operator (bottom). Both MUTAN and our fusion operator take the features $M_r \tilde{\mathbf{q}}$ and $N_r \tilde{\mathbf{v}}$ as input. MUTAN approximates the Tucker decomposition shown in Figure 1 by constraining the bilinear interaction between the vectors $\tilde{\mathbf{q}}$ and $\tilde{\mathbf{v}}$ to be of rank R . Note that while \mathcal{T}_c in Figure 1 is a learned tensor whose parameters implicitly describe the bilinear interaction between $\tilde{\mathbf{q}}$ and $\tilde{\mathbf{v}}$, here the parameters of M_r and N_r are separate and the bilinear interaction is due to the Hadamard product. Our fusion operator generalizes MUTAN first by allowing different nonlinearities f_{rq} and f_{rv} to act on the features $M_r \tilde{\mathbf{q}}$ and $N_r \tilde{\mathbf{v}}$. The result is then composed with an additional learned nonlinearity in the form of a neural network, producing a set of R output features, as in MUTAN after the Hadamard product step $M_r \tilde{\mathbf{q}} \odot N_r \tilde{\mathbf{v}}$. In the case of MUTAN, the R output feature vectors are combined by element-wise summation, whereas in our fusion operator the R feature vectors are combined by applying a tree of binary operators \oplus_b , as described by Algorithm 1.

Therefore, MUTAN is a special case of the Tucker decomposition in Equation 3, as given by Equation 5, where \mathbf{y} is the prediction output of the fusion operator:

$$\mathbf{y} = \mathcal{T}_c \times_1 \mathbf{q}^\top W_{\mathbf{q}} \times_2 \mathbf{v}^\top W_{\mathbf{v}} \times_3 W_o \quad (5)$$

In the following, we derive from the Equation 5 form of MUTAN an expression for MUTAN that can be generalized to a family of fusion operators, over which a variety of specific instantiations can be chosen and evaluated. Throughout the derivation, $\tilde{\mathbf{q}}$ is shorthand for $\mathbf{q}^\top W_{\mathbf{q}}$, and $\tilde{\mathbf{v}}$ represents $\mathbf{v}^\top W_{\mathbf{v}}$.

Referring to $\mathcal{T}_c \times_1 \mathbf{q}^\top W_{\mathbf{q}}$ as $\mathcal{T}_c^{\mathbf{q}}$, each element of the matrix $\mathcal{T}_c^{\mathbf{q}}$ in terms of elements of $\tilde{\mathbf{q}}$ and \mathcal{T}_c is $\mathcal{T}_c^{\mathbf{q}}[j, k] = \sum_{i=1}^{t_q} \mathcal{T}_c[i, j, k] \cdot \tilde{\mathbf{q}}[i]$, which follows from the definition of the n -mode tensor product.

Similarly, we expand the elements of the vector $\mathcal{T}_c^{\mathbf{qv}} = \mathcal{T}_c^{\mathbf{q}} \tilde{\mathbf{v}}$ in terms of elements of $\tilde{\mathbf{q}}$ and $\tilde{\mathbf{v}}$, and slices of \mathcal{T}_c .

$$\begin{aligned} \mathcal{T}_c^{\mathbf{qv}}[k] &= \sum_{j=1}^{t_v} \mathcal{T}_c^{\mathbf{q}}[j, k] \cdot \tilde{\mathbf{v}}[j] \\ &= \sum_{j=1}^{t_v} \left(\sum_{i=1}^{t_q} \mathcal{T}_c[i, j, k] \cdot \tilde{\mathbf{q}}[i] \right) \cdot \tilde{\mathbf{v}}[j] \\ &= \tilde{\mathbf{q}}^\top \mathcal{T}_c[:, :, k] \tilde{\mathbf{v}} \end{aligned} \quad (6)$$

The constraint enforced by [8] in MUTAN is that each slice of the core tensor, i.e., $\mathcal{T}_c[:, :, k]$, must be of rank R , and therefore a sum of matrices each given by an outer product of vectors. Therefore,

$$\mathcal{T}_c[:, :, k] = \sum_{r=1}^R \mathbf{m}_r^k \otimes \mathbf{n}_r^k = \sum_{r=1}^R \mathbf{m}_r^k \mathbf{n}_r^{k^\top}, \quad (7)$$

where $\mathbf{m}_r^k \in \mathbb{R}^{t_q \times 1}$ and $\mathbf{n}_r^k \in \mathbb{R}^{1 \times t_v}$. Substituting Equation 7 into the last line of Equation 6 gives:

$$\begin{aligned} \mathcal{T}_c^{\mathbf{qv}}[k] &= \tilde{\mathbf{q}}^\top \left(\sum_{r=1}^R \mathbf{m}_r^k \mathbf{n}_r^{k^\top} \right) \tilde{\mathbf{v}} \\ &= \sum_{r=1}^R (\tilde{\mathbf{q}}^\top \mathbf{m}_r^k) (\mathbf{n}_r^{k^\top} \tilde{\mathbf{v}}), \end{aligned} \quad (8)$$

where each term in the sum is a scalar. Equation 8 states that $\mathcal{T}_c^{\mathbf{qv}}$ is the sum over $r \in \{1, \dots, R\}$ of matrix-vector element-wise products $M_r \tilde{\mathbf{q}} \odot N_r \tilde{\mathbf{v}}$, i.e.,

$$\mathcal{T}_c^{\mathbf{qv}} = \sum_{r=1}^R M_r \tilde{\mathbf{q}} \odot N_r \tilde{\mathbf{v}}. \quad (9)$$

In Equation 9, $M_r \in \mathbb{R}^{t_o \times t_q}$ and $N_r \in \mathbb{R}^{t_o \times t_v}$ are learned matrices, whose rows are the vectors \mathbf{m}_r^k and \mathbf{n}_r^k , respectively.

We have presented an equivalent form of the MUTAN fusion operator in Equation 9, of which the MLB fusion operator of [7] is a special case where $R = 1$. In this paper, we propose a further generalized extension to Equation 9, by allowing the fusion operator to contain the following transformations:

- A unique pair of unary activation functions (f_{rq}, f_{rv}) that can wrap the individual factors before the Hadamard

product. We refer to the combination of unique pairs of nonlinearities as Nonlinearity Ensembling.

- A sequence of L neural network layers ϕ_l composing a feedforward neural network module Φ that can take the features produced by the bilinear interaction $M_r \tilde{\mathbf{q}} \odot N_r \tilde{\mathbf{v}}$ as input, thereby introducing additional nonlinearity into the fusion operator.
- Skip connections [9], [17] may exist between the inputs to the fusion operator, the outputs of any given neural network layer ϕ_j in the fusion operator, and the inputs to any other neural network layer ϕ_k , or the final output of the fusion operator.
- The sum over R terms in Equation 9 is generalized to arbitrary binary relations $\oplus_b(\cdot, \cdot)$. Each binary relation \oplus_b is associated with a set $\{\mathcal{T}_r^{\mathbf{q}\mathbf{v}}\}_b$ corresponding to an element of a partition of the outputs $\mathcal{T}_r^{\mathbf{q}\mathbf{v}}$ from the R branches of the fusion operator, before those branches are joined. $\mathcal{T}_r^{\mathbf{q}\mathbf{v}}$ is defined according to Equation 10:

$$\mathcal{T}_r^{\mathbf{q}\mathbf{v}} = \Phi_r(f_{rq}(M_r \tilde{\mathbf{q}}) \odot f_{rv}(N_r \tilde{\mathbf{v}})). \quad (10)$$

There is also an ordering over the binary operations such that \oplus_b form a sequence $(\oplus_b)_{b=1}^B$, where B represents the total number of distinct binary operators and is equal to the number of subsets in the partition $\{\mathcal{T}_r^{\mathbf{q}\mathbf{v}}\}_b$.

The sequence $(\oplus_b)_{b=1}^B$ is applied recursively to the partitions $\mathbb{B}_b := \{\mathcal{T}_r^{\mathbf{q}\mathbf{v}}\}_b$ according to Algorithm 1.

The generalization over binary operators allows for binary operations besides addition to be applied to the $\mathcal{T}_r^{\mathbf{q}\mathbf{v}}$ output from each branch of the fusion operator, and also allows definition of precedence rules so that binary operators can be applied in a defined order. The fusion operator in Equation 9 is the special case of the generalized fusion operator where $B = 1$, $\oplus_1 = +$, and \mathbb{B}_1 is the entire set of branch outputs $\{\mathcal{T}_r^{\mathbf{q}\mathbf{v}}\}$.

Algorithm 1 Recursively applies the binary operator sequence $(\oplus_b)_{b=1}^B$ to the sequence $(\mathbb{B}_b)_{b=1}^B$ of elements of a partition of the set of outputs from each of the R branches of the generalized fusion operator. The $\text{IDENTITY}(\oplus)$ function returns the identity for the binary operator \oplus .

```

1: function APPLYBINOPSEQUENCE( $(\mathbb{B}_b)_{b=1}^B, (\oplus_b)_{b=1}^B$ )
2:    $v \leftarrow \text{IDENTITY}(\oplus_1)$ 
3:   for all  $b \in \{1, \dots, B\}$  do
4:      $v_b \leftarrow \text{IDENTITY}(\oplus_b)$ 
5:     for all  $\mathcal{T}_r^{\mathbf{q}\mathbf{v}} \in \mathbb{B}_b$  do
6:        $v_b \leftarrow v_b \oplus_b \mathcal{T}_r^{\mathbf{q}\mathbf{v}}$ 
7:     end for
8:      $v \leftarrow v \oplus_b v_b$ 
9:   end for
10:  return  $v$ 
11: end function

```

Our generalized fusion operator is compared alongside MUTAN in Figure 2.

IV. EXPERIMENTS

In this section, we instantiate specific models based on the generalized fusion operator described by Algorithm 1. We individually test the specific extensions for a generalized fusion operator, as described in Section III-B. We then demonstrate the degree to which the extensions’ performance gains are complementary.

In all of the following experiments, the Adam optimizer [18] is used to train each model with a learning rate of 10^{-4} . The models are trained for 100 epochs. For the validation set, models with the best validation accuracy are selected. For the test-dev set, the model parameters used to generate test-dev predictions correspond to the early-stopping epoch determined from the validation set.

Following the hyperparameter settings of [8], the number of branches used in the fusion operator is $R = 5$. The dimensionality of the question vector \mathbf{q} is the default for uni-skip Skip-Thought Vectors $d_q = 2400$, while the visual vector \mathbf{v} is the $d_v = 2048$ dimensional output of a ResNet. Question and visual features are projected into a $t_q = t_v = 310$ dimensional vector space before being reprojected into a $t_o = 510$ dimensional vector space where \mathbf{q} and \mathbf{v} are combined by Hadamard product. The batch size used in our experiments is 128.

A. Nonlinearity Ensembling (NE)

To test the contribution of using a variety of activation functions per branch of the fusion operator, we first conducted a grid search over possible combinations where each f_{rq} and f_{rv} was drawn uniformly from the following set of candidate nonlinearities: identity function, leaky ReLU [19], SeLU [20], sigmoid, and tanh. We subsampled the VQA 1.0 dataset and ran a grid search with each run lasting only 5 epochs in order to quickly observe many combinations of nonlinear activation function pairs.

From the grid search, we observed the pattern that the stronger nonlinearity pair combinations used SeLU as the visual vector activation function, while using a variety of different activation functions on the question vector. Therefore, to test Nonlinearity Ensembling, we used branches where the visual vectors always used the SeLU nonlinearity, and the branches used one of each activation function on the question vector.

We propose that the diversity in the activation function on the question vector decreases the correlation between the branches, hence improving the ensembling effect of summing the branches’ predictions together.

B. Post-fusion neural networks with skip connections

In order to allow for a nonlinear function to act on the bilinear features extracted by the Hadamard product between $M_r \tilde{\mathbf{q}}$ and $N_r \tilde{\mathbf{v}}$, we propose adding a neural network Φ_r to the fusion operator. We embed a “tiny” neural network in the fusion operator analogous to how Network in Network [21] embeds a tiny neural network in a convolution.

In our implementation, Φ_r consists of a sequence of blocks of three feedforward layers where the activation function for each layer matches that of f_{rq} . There is a skip connection from the input, and from every third layer, to the output.

C. Feature Gating (FG) and Polarity Swap (PS)

Algorithm 1 introduces a method of generalizing the sum operation over fusion operator branch outputs $\mathcal{T}_r^{\text{qv}}$ to an ordered set of binary operations. We test two particular instantiations of Algorithm 1 where $B = 2$, $\oplus_1 = +$, $\oplus_2 = \odot$ and $|\mathbb{B}_2| = 1$, i.e. $R-1$ of the branch outputs $\mathcal{T}_r^{\text{qv}}$ are summed and then element-wise multiplied by the remaining branch output.

Assume that the branch output that gets multiplied with the sum of the other branch outputs is $\mathcal{T}_R^{\text{qv}}$. The output of $\mathcal{T}_R^{\text{qv}}$ is first squashed by a nonlinearity f before being multiplied into the sum over \mathbb{B}_1 .

In the case of our first experiment, the squashing nonlinearity is the logistic function f_{sigmoid} , which independently squashes the output $f_{\text{sigmoid}}(\mathcal{T}_R^{\text{qv}})$ into the range $(0, 1)$. The effect of multiplying by this squashed output is therefore to turn each feature on or off, so we refer to the first experiment as Feature Gating.

The squashing nonlinearity used in the second experiment is $\tanh f_{\text{tanh}}$, which has the effect of squashing $f_{\text{tanh}}(\mathcal{T}_R^{\text{qv}})$ to the range $(-1, 1)$. We refer to the second experiment as Polarity Swap, since negative features can be conditionally swapped to positive and vice-versa.

Figure 3 demonstrates an example instantiated fusion operator that makes use of the Feature Gating idea, and implements the Feature Gating experiment described above. In Figure 3, the number of branches is set to $R = 3$ for clarity, while in the experiments of Table I, the models have $R = 5$ branches.

V. RESULTS

In Table I, we compare performance improvements between different instantiations of the generalized fusion operator described in Equation 10 and Algorithm 1, which are discussed in Section IV. We use the VQA 1.0 validation set to compare the effect on the performance of fusion operators of adding Nonlinearity Ensembling, as well as Feature Gating and Polarity Swap, independently. We chose to first investigate these static components of the fusion operator design before fixing them while investigating possible post-fusion neural networks. Since the neural network is a learned component of the architecture, it has to adapt to the static components during training, and hence the optimal hyperparameters of the neural network may vary depending on the choice of static components in the model.

The Nonlinearity Ensembling component improves the fusion operator’s performance on the VQA 1.0 validation set, and this improvement stacks with the performance improvement achieved from Feature Gating. Furthermore, the performance of Feature Gating is better compared to Polarity Swap, when each is combined with Nonlinearity Ensembling.

We find that the improvements from the Feature Gating and Polarity Swap model elements do not stack. We combine the

TABLE I
AN ABLATION STUDY ON NONLINEARITY ENSEMBLING, FEATURE GATING, AND POLARITY SWAP.

Model	VQA 1.0 val
MUTAN [8]	61.54
Nonlinearity Ensembling (NE)	61.66
Feature Gating (FG)	61.72
NE + Polarity Swap (PS)	61.77
NE + FG	61.86

ideas by using one branch each to multiply by a vector of tanh and sigmoid outputs. The combined model performs slightly worse than the Polarity Swap model by itself, which in turn performs worse than the Feature Gating model.

Therefore, the best performing combination amongst Nonlinearity Ensembling, Feature Gating and Polarity Swap occurs from using the Nonlinearity Ensembling and Feature Gating together.

Building on the best model based on the ablation study of Table I, we use the more challenging VQA 2.0 validation set to evaluate different post-fusion neural network architectures. We find that a post-fusion neural network with six layers and 128 hidden units per layer outperforms the NE + FG model by a margin of 0.53 percentage points, improving the VQA 2.0 validation OpenEnded accuracy (as defined in [15]) from 60.57% to 61.1%. We find that with the low number of 128 hidden units, dropout is detrimental to the accuracy, and the best model does not use dropout.

In Table II, we evaluate our best model on the VQA 2.0 test-dev and test-std sets, and compare to previous state of the art models upon which our work is based, as well as to the best models of [22], the winners of the 2017 VQA challenge. We find that our best model achieves an absolute percentage point improvement of 1.1% over the strong baseline of [8]. We note that the improvement in OpenEnded accuracy of our model on the test-dev set is significantly larger in magnitude when compared to the improvement of [8] over [6]. We attribute our relatively large improvement in accuracy to the introduction of nonlinearities in the fusion operator. The nonlinearities both allow the fusion operator to ensemble nonlinear functions of the input features (via Nonlinearity Ensembling), and to model nonlinear relationships between the bilinear features extracted by the Hadamard product (via the post-fusion neural networks).

When comparing our model’s performance to that of the models of [22] in Table II, we note that the best performing models of [22] gain a significant performance boost from using superior image features for the VQA task. In particular, [22] use bottom-up attention [23], which makes use of a Faster R-CNN [24] pipeline, to obtain features from object proposal regions of an image. Bottom-up attention features improve the models of [22] by $\approx 3\%$ absolute percentage points on average, and since our contribution focuses solely on improving the fusion operator, our model should gain similar improvements from using bottom-up attention features.

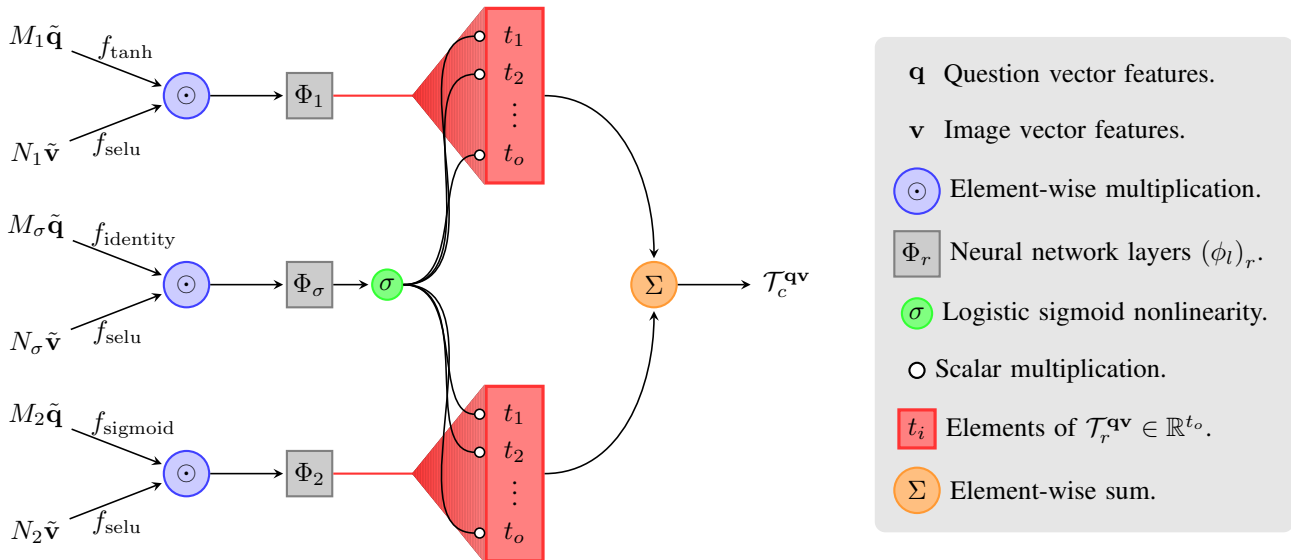


Fig. 3. An example network using the Feature Gating neural network component, where each node represents a computation and the arrows represent the forward flow of information. The question and image feature vectors \mathbf{q} and \mathbf{v} are shared inputs to all branches. The Φ_r nodes represent post-fusion feedforward neural networks with skip connections. The logistic sigmoid node σ squashes output features $\mathcal{T}_\sigma^{\mathbf{q}\mathbf{v}}$ from Φ_σ to a vector of values in $(0, 1)$. The output from σ is element-wise multiplied with all other $\mathcal{T}_r^{\mathbf{q}\mathbf{v}}$ features from each branch, effectively turning on or off each feature channel. The resultant gated $\mathcal{T}_r^{\mathbf{q}\mathbf{v}}$ features are summed to become $\mathcal{T}_c^{\mathbf{q}\mathbf{v}}$, features that are input into a predictive layer to score the most common answers to questions from the VQA task.

The multimodal fusion operator used in [22] is a Hadamard product, as in MLB.

VI. CONCLUSION AND FUTURE WORK

We presented a generalization of the MUTAN operator aimed at fusing multi-modal representations. We demonstrated the expressibility of the operator, showing that it could ensemble a variety of different nonlinearities, implement neural networks post-ensembling, and generalize MUTAN's sum-based reduction to hierarchical fusion with arbitrary binary operators. The few configurations we tested demonstrated significant gains relative to MUTAN and MCB on the VQA 2.0 task. However, the most promise lies not in choosing a configuration by hand, but leveraging this generalization as a design space for architecture search by reinforcement learning or other methods. This is the focus of future work.

TABLE II
A COMPARISON WITH THE STATE OF THE ART OF OUR BEST SINGLE MODEL ON THE VQA 2.0 TEST-DEV AND TEST-STD SETS.

Model	VQA 2.0 test-dev				VQA 2.0 test-std			
	All	Y/N	Number	Other	All	Y/N	Number	Other
MCB [6] as reported in [15]	61.96	78.41	38.81	53.23	62.27	78.82	38.28	53.36
MUTAN [8] as trained and evaluated by us	63.13	80.7	39.4	53.55	—	—	—	—
ResNet features 7×7 (single) [22]	62.07	79.20	39.46	52.62	62.27	79.32	39.77	52.59
Bottom-up attention image features, adaptive K (single) [22]	65.32	81.82	44.21	56.05	65.67	82.20	43.90	56.26
Ours (single)	64.22	81.19	40.95	55.05	64.64	81.62	41.19	55.22

REFERENCES

- [1] B. Zoph and Q. V. Le, “Neural architecture search with reinforcement learning,” in *5th Int. Conf. on Learning Representations (ICLR)*, 2017.
- [2] I. Bello, B. Zoph, V. Vasudevan, and Q. V. Le, “Neural optimizer search with reinforcement learning,” in *Int. Conf. on Machine Learning (ICML)*, 2017.
- [3] P. Ramachandran, B. Zoph, and Q. Le, “Searching for activation functions,” *arXiv preprint arXiv:1710.05941*, 2017.
- [4] H. Liu, K. Simonyan, O. Vinyals, C. Fernando, and K. Kavukcuoglu, “Hierarchical representations for efficient architecture search,” *Int. Conf. on Learning Representations (ICLR)*, 2018.
- [5] G. Malkomes, C. Schaff, and R. Garnett, “Bayesian optimization for automated model selection,” in *Advances in Neural Information Processing Systems 29 (NIPS)*, 2016, pp. 2900–2908.
- [6] A. Fukui, D. H. Park, D. Yang, A. Rohrbach, T. Darrell, and M. Rohrbach, “Multimodal compact bilinear pooling for visual question answering and visual grounding,” in *Proc. 2016 Conf. on Empirical Methods in Natural Language Processing (EMNLP)*, 2016, pp. 457–468.
- [7] J.-H. Kim, K. W. On, W. Lim, J. Kim, J.-W. Ha, and B.-T. Zhang, “Hadamard Product for Low-rank Bilinear Pooling,” in *The 5th Int. Conf. on Learning Representations (ICLR)*, 2017.
- [8] H. Ben-younes, R. Cadene, M. Cord, and N. Thome, “MUTAN: Multimodal tucker fusion for visual question answering,” in *IEEE Int. Conf. on Computer Vision (ICCV)*, 2017.
- [9] K. He, X. Zhang, S. Ren, and J. Sun, “Deep residual learning for image recognition,” in *Proc. IEEE Conf. on Computer Vision and Pattern Recognition (CVPR)*, 2016, pp. 770–778.
- [10] R. Kiros, Y. Zhu, R. Salakhutdinov, R. S. Zemel, A. Torralba, R. Urtasun, and S. Fidler, “Skip-thought vectors,” in *Advances in Neural Information Processing Systems 28 (NIPS)*, 2015, pp. 3294–3302.
- [11] Y. Gao, O. Beijbom, N. Zhang, and T. Darrell, “Compact bilinear pooling,” in *Proc. IEEE Conf. on Computer Vision and Pattern Recognition (CVPR)*, 2016, pp. 317–326.
- [12] M. Charikar, K. Chen, and M. Farach-Colton, “Finding frequent items in data streams,” in *Proc. 29th Int. Colloquium on Automata, Languages and Programming*, 2002, pp. 693–703.
- [13] T. G. Kolda and B. W. Bader, “Tensor decompositions and applications,” in *SIAM review*, 2009, pp. 455–500.
- [14] S. Antol, A. Agrawal, J. Lu, M. Mitchell, D. Batra, C. L. Zitnick, and D. Parikh, “VQA: Visual Question Answering,” in *Int. Conf. on Computer Vision (ICCV)*, 2015.
- [15] Y. Goyal, T. Khot, D. Summers-Stay, D. Batra, and D. Parikh, “Making the v in vqa matter: Elevating the role of image understanding in visual question answering,” in *Proc. IEEE Conf. on Computer Vision and Pattern Recognition (CVPR)*, 2017.
- [16] O. Russakovsky, J. Deng, H. Su, J. Krause, S. Satheesh, S. Ma, Z. Huang, A. Karpathy, A. Khosla, M. Bernstein *et al.*, “Imagenet large scale visual recognition challenge,” in *Int. Journal of Computer Vision*, 2015, pp. 211–252.
- [17] R. K. Srivastava, K. Greff, and J. Schmidhuber, “Training very deep networks,” in *Advances in Neural Information Processing Systems 28 (NIPS)*, 2015, pp. 2377–2385.
- [18] D. P. Kingma and J. Ba, “Adam: A method for stochastic optimization,” in *3rd Int. Conf. on Learning Representations (ICLR)*, 2015.
- [19] A. L. Maas, A. Y. Hannun, and A. Y. Ng, “Rectifier nonlinearities improve neural network acoustic models,” in *Int. Conf. on Machine Learning (ICML)*, 2013.
- [20] G. Klambauer, T. Unterthiner, A. Mayr, and S. Hochreiter, “Self-normalizing neural networks,” in *Advances in Neural Information Processing Systems (NIPS)*, 2017, pp. 972–981.
- [21] M. Lin, Q. Chen, and S. Yan, “Network in network,” *Int. Conf. on Learning Representations (ICLR)*, 2014.
- [22] D. Teney, P. Anderson, X. He, and A. v. d. Hengel, “Tips and tricks for visual question answering: Learnings from the 2017 challenge,” *arXiv preprint arXiv:1708.02711*, 2017.
- [23] P. Anderson, X. He, C. Buehler, D. Teney, M. Johnson, S. Gould, and L. Zhang, “Bottom-up and top-down attention for image captioning and vqa,” *arXiv preprint arXiv:1707.07998*, 2017.
- [24] S. Ren, K. He, R. Girshick, and J. Sun, “Faster r-cnn: Towards real-time object detection with region proposal networks,” in *Advances in Neural Information Processing Systems (NIPS)*, 2015, pp. 91–99.